

**MJO Teleconnection Patterns and their
Effect on Extratropical Cyclone Activity in
the Mid-latitudes**

by

Angelica C. Soria

A thesis submitted in partial fulfillment of the
requirements for the degree of

Master of Science

Atmospheric and Oceanic Sciences

at the

UNIVERSITY OF WISCONSIN-MADISON

2021

Table of Contents

Acknowledgments

Abstract

1 Introduction

1.1: MJO Internal Dynamics

1.2: MJO Teleconnections

1.3: Effects on Extratropical Cyclone Tracks

1.4: MJO Teleconnections & Severe Weather Impacts

2 Methodology

3 Results

3.1 500-hPa Geopotential Height Anomalies

3.2: Frequency Climatology

3.3 Frequency Composited by MJO Phase

3.4 Intensity Climatology

3.5 Intensity Composited by MJO Phase

4 Summary & Conclusion

5 Future Work

References

Acknowledgements

First off, I want to thank my thesis committee made up of my advisor, Stephanie Henderson, Jon Martin, and Angel Adames, for their feedback and time they gave to me. Getting into graduate school was a goal I had set for myself. I knew I wanted a master's degree but I had no idea that my journey would look like this. Before coming to the University of Wisconsin-Madison, I really hadn't had much research experience. I never knew what my research interests were or if there was a project I could be interested in enough to write about and work on for the next couple of years.

Fortunately, I was really lucky and was chosen by the best advisor to come be a part of her new research group. It was Stephanie Henderson's first semester as an advisor but I could already tell she was going to be awesome. I could not have done any of this research without her teaching me about the MJO and helping me find a topic I was passionate about. Through the stressful times and exciting coding breakthroughs, she was there for me. She taught me so much about how to read other people's research and how to present my own findings and basically how to be a good research assistant. She even helped me prepare for my dream job interview and was one of the main reasons I received a job offer from the National Weather Service. I included her as one of my references on my job application and was told that she had nothing but good things to say about me and my work ethic. Her review weighed heavily in the decision process and the hiring committee liked what she had to say and I was chosen! Even through a pandemic and me moving across the country for my dream job, she found ways to help me and made sure I was still moving right along with my research. I can't thank her enough for everything she's done for me that past couple of years and even

on days that I really didn't feel like coding or writing, I knew how hard we both had worked on this research project and I wanted to finish it and make her proud.

The University of Wisconsin AOS Department was so fun to be a part of but unfortunately my experience on campus was cut short due to the pandemic. This pandemic has been very stressful and some days would drain all of my motivation to focus on school work when I felt there were bigger things happening in the world. There were times I was so stuck on coding and so far away from school that I wanted to give up. Stephanie and Pete Pokrandt helped me with me with coding and getting my VPN settled so that I could work from home. But, one of the people who helped me the most through all my errors and helped me to format my plots and always listened to my presentations, was my best friend Jerrold Acdan. Not sure I could've survived graduate school without him. He would work with me for hours on coding and was so patient with me as I started learning python. Just about everyone in the graduate student program at the University of Wisconsin-Madison helped me in some way or another. Whether it was in class or in our research group, I've learned a lot from a lot of other students. I am forever thankful for the friendships I made in Wisconsin and love the little friend group I made while I was there and they all had their own little parts in helping me with my research.

After receiving my job offer, moving to Texas to start my dream career was exciting yet very overwhelming in addition to finishing my master's research. Luckily, my new office brought along a new friend group for me as well. I am so thankful for their constant encouragement and interest in my research. It makes me excited to talk them about my findings and teach them more about the MJO. Everyone at WFO Brownsville

has been nothing but supportive and patient with me while I try to finish my master's and also learn how to do a new job. I've made some really good friends here already and couldn't have adjusted to the move or the new job as quickly without them.

Lastly, my family and friends from home have definitely seen me struggle through this master's degree. I am very thankful for their constant push for me to always achieve more and to never give up on the goals I have set for myself. I couldn't have finished this degree without them and appreciate them listening to me present my research even if they had no idea what I was talking about! Very grateful for my amazing support system and everyone who has helped me on my journey along the way.

Abstract

This study analyzes the Madden-Julian Oscillation teleconnection pattern and its effect on extratropical cyclone behavior in North America for the spring season: March, April, May, and June (MAMJ). The cyclone characteristics that were focused on were modulations in cyclone movement, frequency, and intensity. Kevin Hodges' (1999) tracking algorithm was used to quantify the extratropical cyclone tracks. To incorporate the MJO teleconnection patterns, daily RMM indices were used to composite the cyclone data by MJO phase. The influence of the MJO's deep tropical convection gets transferred by Rossby waves in ways of teleconnection patterns which changes the large scale dynamics over North America. In addition to using the tracking algorithm, reanalysis ERA5 data was used to analyze 500-hPa geopotential height to see the effects of the teleconnection patterns on large scale dynamics in accompaniment with the modulation of extratropical cyclone tracks. The convection shifts the storm tracks which changes the frequency and movement of the cyclones. Depending on which phase the MJO is in, this also affects the intensity of the cyclones over North America.

Chapter 1

Introduction

The Madden-Julian Oscillation (MJO) is an organized convective system that propagates eastward in the tropics near the equator from the Indian Ocean to the western Pacific at about 5 ms^{-1} for an intraseasonal time period of 30-90 days (Madden and Julian 1972; Weickmann et al. 1985; Knutson et al. 1986). The influence of the MJO's convection gets transported eastward by Rossby waves which are called teleconnection patterns. These teleconnection patterns affect the sub-tropical jet which changes the mean flow (Guo et al., 2017). The changes in the large scale dynamics modulate the extratropical cyclone storm track by shifting them north or southward and also changing their intensities depending on their location in the Pacific (Guo et al., 2017). These teleconnections can contribute to atmospheric rivers, blocking highs, modulations in the extratropical cyclone tracks, and can create favorable environments for severe weather. This research is focused on MJO teleconnections and its impacts on extratropical cyclone tracks during boreal Spring. Results show that storm track frequency and intensity are modulated by the MJO from March – June (MAMJ) and this can lead to modulations in weather patterns across North America as well. Previous studies have mostly focused on the MJO during boreal winter. The motivation behind this study is to conduct research on the MJO during MAMJ because the change in seasonality affects the intensity of the MJO and can be useful when considered in long-term forecasting. Using the MJO as a guide in a forecast can increase its skill which will in turn, improve forecast predictability during the severe weather season.

1.1 MJO Internal Dynamics

The MJO is an eastward propagating center of strong convection and precipitation surrounded by weaker suppressed convection on the west and eastern sides (Zhang, 2005). The MJO varies seasonally and interannually which leads to irregular activity and differences in spectral peaks (Zhang, 2005). The chaotic activity within the MJO is aided by Kelvin and Rossby wave interactions (Lyu et al., 2021). The eastward and westward propagation of these waves, as well as the MJO's own convection, acts to suppress and enhance the intensity of the MJO as well as change its speed (Lyu et al., 2021). According to Lyu et al. (2021), the suppressed and enhanced stages of the MJO affects the Kelvin and Rossby waves around it. A suppressed MJO will create an enhanced Kelvin wave and a suppressed Rossby wave. The Kelvin wave westerlies counteract the Rossby wave easterlies and this difference in wind shear strengthens the boundary layer in the convergence zone east of the MJO which helps to move it east (Lyu et al., 2021). Westerly and easterly winds on both sides of the deep tropical convection center work to overturn the zonal circulation throughout all levels of the atmosphere and drive the air-sea coupling needed to sustain the eastward propagation (Zhang, 2005).

The eastward movement is much slower than a Kelvin wave as they usually move about 15 ms^{-1} (Wheeler and Kiladis, 1999; Straub and Kiladis, 2002). Even though the MJO convection stays mostly in the Indo-Pacific region, its impacts on the upper atmosphere can reach across the globe. The winds and associated perturbations in

sea-level pressure travel as dry Kelvin waves across the Pacific once the MJO is decoupled to convection, moving at about 30 ms^{-1} (Zhang, 2005). The speed and intensity of these Kelvin waves tend to vary based on what phase the MJO is in and if it is in an active or inactive state (Chen & Wang, 2018; Kim et al., 2014).

The MJO has also been known to trigger monsoon events and El Niño-Southern Oscillation (ENSO) events. Strong MJO events can have an effect on the intensity of an ENSO pattern. It can enhance or suppress the severity of the current ENSO by affecting the SST's in the western Pacific Ocean. The change in SST's is thought to be caused by surface latent heat flux or low-level moisture convergence (Zhang 2005). If positive anomalous SST's are present, this eastward moving anomalous warm pool allows for the MJO to move further towards the central Pacific (Anyamba and Weare, 1995; Hendon et al., 1999). The MJO has the biggest impact when it is in an active phase during ENSO warm events (Chang et al., 1996; Penland, 1996). Oceanic Kelvin waves produced by the MJO move eastward, suppressing the thermocline and causing the water in the area to remain warm due to lack of upwelling. The stochastic forcing of the MJO is not the reason ENSO exists, but is an important modulator of variability when it comes to ENSO predictability.

1.2 MJO Teleconnections

The MJO affects many weather phenomena based on its intensity and location by forcing Rossby waves, or teleconnection patterns. These teleconnection patterns are an atmospheric circulation response to the latent heat released from the convection of the MJO (Guo et al., 2017). Extratropical cyclones are important to track because they

transport tropical moisture (Guo et al., 2017). The movement and phase change of moisture can change the large scale dynamics through the teleconnection patterns. Understanding how the MJO's convection is transported through its teleconnection patterns can make it important for forecasting. These teleconnection patterns take about one to two weeks to reach North America. Monitoring the MJO for enhanced or suppressed activity can be telling of whether or not there will be a drastic change in weather pattern in the next 10-15 days which can help strengthen intraseasonal forecasting skill.

The oscillating moisture and convection can affect extratropical weather in a variety of ways. For example, the MJO has the ability to change the path and intensity of winter extratropical cyclones (e.g. Guo et al., 2017). This may lead to changes in enhanced or reduced storm tracks during the winter (Guo et al., 2017) or severe weather outbreaks in certain areas of the country (Barrett and Gensini, 2013). Modulation of the storm tracks due to the teleconnection patterns can also create blocking high patterns. A blocking high is a high pressure system that remains over the same area for over a certain period of time. Based on previous studies from Moore et al. (2010) and Henderson et al. (2016), the MJO's teleconnection patterns affect the location of the subtropical-jet stream which leads to Rossby wave breaking. This Rossby wave breaking often triggers the North American Oscillation (NAO) to transition into a positive phase which leads to a blocking pattern over Europe (Henderson et al., 2016). These blocking patterns can lead to drought conditions, cold snaps, or even interfere with the precipitation for that area.

This study examines how MJO teleconnection patterns impact extratropical cyclone tracks in the spring season. MJO teleconnection patterns, while strongest in the winter season, still impact North America during all times of the year. The spring season is important because it is associated with severe weather in the Plains and southern regions of the United States. Severe weather can be very costly to those communities. Studying one season can be beneficial in determining what happens with the cyclone tracks and in which MJO phase are the paths affected the most.

The MJO is typically very active during the winter season months of December-February. However, the MJO can affect weather in North America during the spring months as well. Baggett et al. (2018) examined MJO impacts during the spring severe weather season. The study showed that the MJO impacts the severe weather environmental conditions in certain parts of the United States such as the Plains and Ohio River Valley. The paper showed that certain MJO phases would enhance or suppress the probability of large hail, flash flooding, or the possibility of tornadoes. The work supports that MJO indices can be a helpful tool in forecasting severe weather outbreaks and may help increase lead time since the MJO is an intraseasonal phenomena.

Using the MJO as a predictor may help increase the forecast lead time of weather patterns in the United States during MAMJ. For example, for severe weather, forecasters currently suffer a sub-seasonal to seasonal forecast gap with lead times of 2-5 weeks (Baggett et al., 2018). The National Oceanic and Atmospheric Administration's Storm Prediction Center issues their outlooks for 0-8 days and their Climate Prediction Center issues their seasonal outlooks with lead times of 1 month

(Baggett et al., 2018). Using the MJO's current state can be telling of how favorable the conditions are for severe weather over North America (Barrett and Gensini, 2013). In this study, the MJO is a major factor in cyclone direction and frequency. Studying MJO teleconnection patterns and their impacts can improve forecasts especially in the medium range time period.

For years, cyclone movement has been analyzed by their tracks, intensity, and longevity. In the mid 1990's, Kevin Hodges created a cyclone algorithm to monitor cyclone behavior (Hodges 1999). This algorithm takes a set minimum sea level pressure and tracks the center of the cyclone on a mesh grid. Each track follows certain constraints in order to only include strong, long-lasting cyclones. These tracks provide a visual representation of where and how many cyclones occur in the northern hemisphere. This tracking algorithm is used here to examine how the MJO impacts extratropical cyclone tracks on a daily time scale.

1.3 Effects on Extratropical Cyclone Tracks

Deng et al. (2011) conducted research for boreal winter on the MJO's convection and its modulation of northern Pacific storm tracks. OLR data and 925-200-hPa geopotential height averaged synoptic eddy kinetic energy (SEKE) data were used to focus on the eddy-mean flow interactions between synoptic scale flow and intraseasonal flow. They found that when the MJO's convection is centered around the western Pacific or over the Maritime Continent, the convection did affect the large scale dynamics over the northern Pacific and modulated the storm track anomalies (Deng et al., 2011). When the deep tropical convection was situated over the western Pacific, this

lead to anomalous low pressure in the northern Pacific and anomalous high pressure just to its south. When the convection was over the Maritime Continent, the pattern was flipped and anomalous high pressure was situated in the northern Pacific slightly north of the anomalous low pressure (Deng et al., 2011). The changes in extratropical cyclone tracks created a “dry-wet-dry” precipitation pattern that flows northeastward affecting the winter weather over the western portion of the North America (Deng et al., 2011).

Grise et al. (2013) also examined changes in extratropical cyclone tracks during boreal winter but instead, employed the Hodges (1999) tracking algorithm. The study also included impacts from the North Atlantic Oscillation (NAO), ENSO, the Pacific-North American pattern (PNA), and the MJO. These four patterns are all large-scale patterns that can alter climatological extratropical cyclone pathways and intensities. The PNA and NAO patterns are also dependent on the MJO. As mentioned earlier, past research such as Moore et al. (2010) and Henderson et al. (2016) have suggested that the MJO can trigger an NAO or PNA pattern.

The NAO is a north-south shift in the zonal wind maximum over the north Atlantic Ocean in between the Icelandic low and Azores high (Hurrell et al., 2003). The NAO affects extratropical cyclone activity by shifting the tracks according to where the zonal wind maximum is at the time by shifting the North Atlantic jet stream (Hurrell 1995; Grise et al., 2013). A positive phase of the NAO typically leads to low pressure over the north Atlantic and high pressure over the north-central Atlantic (Climate 2012). For the negative phase of the NAO, the high and low pressure centers are flipped. The NAO affects temperature and precipitation over the eastern United States and central Europe (Climate 2012). Positive NAO will bring above average temperatures to the eastern

United States and below average temperatures across Greenland. As well as above average precipitation to northern Europe and below average precipitation to central Europe (Climate 2012). The negative phase of the NAO will flip the temperature and precipitation anomalies across the respective locations (Climate 2012).

As for the PNA, it has four centers which are located in the northeastern Pacific, Gulf of Alaska, northwestern North America, and southeastern United States (Baxter and Nigam 2013). It also has positive and negative phases and those each impact the Northern Hemisphere extratropics differently. The PNA modulates the East Asia jet stream which affects the temperatures and precipitation over North America. For a positive PNA phase, high pressure will linger near Hawaii and low pressure will stay near the southeastern United States (Climate 2012). This leads to above average temperatures in the western half of the United States and below average temperature for the southeastern United States (Climate 2012). For a negative phase of the PNA, the jet is shifted westward which limits the extratropical cyclone activity over the north Pacific (Climate 2012).

The study found that most cyclones occur over the central North Pacific and the North Atlantic Oceans, and in the central plains and Great Lakes over North America. There is generally a lack of storms in the southwestern region of the United States. To relate the tracks to the climate patterns, Grise et al. (2013) used a pentad-mean method on the track data. Next, the anomalies were found and a Monte Carlo test with 1000 random samples was used to find statistical significance. The number of extratropical cyclones over North America changed similarly to the intensity of the teleconnection patterns from the MJO (Grise et al., 2013). As the teleconnection patterns became

stronger (correlated to a stronger MJO phase), the frequency of extratropical cyclones over North America would also increase. The study found that during phase 3 cyclone activity can be seen mostly off the west coast of the United States while phase 4 showed cyclone track anomalies in central Canada (Grise et al., 2013). The last two phases, 5 and 6, had an increase in positive anomalous cyclone development in the Great Lakes region and an increase in positive anomalous cyclosis in the southeastern region. Grise et al. (2013) found that storm tracks during MJO phase 3 and 4 are similar to those during the positive NAO phase. For MJO phases 5 and 6, storm track anomalies related to the negative phase of the PNA. An important finding from their study is that anomalous cyclone tracks occur where anomalous cyclonic wind shear occurs. The wind shear becomes anomalous when the westerly wind is dominant in the upper atmosphere (Grise et al., 2013).

There were many other factors that need to be considered when diagnosing the intraseasonal variability of these tracks. Grise et al. (2013) mentions that sea surface temperatures and the stratosphere circulation change with the season which may also impact the tracks. However, recognizing that the four climate phenomena interact with each other is important in understanding how they affect the weather in North America.

The impact of MJO teleconnections on wintertime extratropical cyclone movement and intensity was examined by Guo et al. (2017) using the Hodges (1999) tracking algorithm and eddy statistics. They too noticed that MJO teleconnection patterns most commonly affected the weather in North America. Their research focused on extended boreal winter (November-April) for a 36-year time period (1979-2014) using ERA-Interim reanalysis 6-hourly data and mean sea level pressure. To define the MJO,

the study used the real-time multivariate MJO (RMM) indices (Wheeler and Hendon 2004) and only used strong MJO events, defined as an RMM amplitude greater or equal to one. Kevin Hodges' tracking algorithm (Hodges 1999) is applied to mean sea level pressure data from ERA5 reanalysis (Hersbach et al., 2020). Hodges' (1999) method consisted of an upper-bound displacement constraint, velocity constraints, and track smoothness constraints. The cyclone constraints were performed on the data to link together similar minimum mean sea level pressure centers (1013 hPa). A smoothing constraint is applied to the minimum mean sea level pressure center points both forward and backwards in time (Hodges 1999). Only cyclone tracks lasting longer than two days were examined with a track length of at least 1000km. The cyclone tracks provide 3 hourly data, latitude and longitude for all cyclone points, and intensity for each point.

The study supplemented this by examining eddy variance using a bandpass-filter (i.e. the 24-h-difference-filtered variance, originally used in Wallace et al. 1988). Guo et al. (2017) states that both techniques have strengths and weaknesses, and using both strengthens their analysis. From these two perspectives, Guo et al. (2017) composited cyclone intensity, cyclone frequency, total column water vapor, and accumulated cyclone activity by MJO phase. For this literature review, only the cyclone intensity, frequency and accumulated activity changes will be discussed, as these same metrics are used in this study.

Cyclone frequency is computed by taking the number of cyclones and divided by the number of days they occurred and converting those values to a percent. In the Northern Hemisphere, Guo et al. (2017) found that the highest frequency of cyclones occurs in the northern Pacific Ocean, North America, and over the northwest Atlantic

Ocean with a peak around 7-10%. Cyclone frequency during MJO phase 1 show positive anomalies in the northern Pacific Ocean and off the east coast of the United States. During phase 2 in the north central Pacific, there is a strong positive anomaly located just north of a strong negative anomaly indicating that the storm track shifts north. There is also a slight eastward shift in the north central Atlantic Ocean. Phases 3 and 4 are associated with a decrease in storm frequency over the central Pacific Ocean. Phase 6 and 7 result in a slight southward shift of the storm track in the central Pacific and during phase 6, there is an area of positive anomalous values on land over the Pacific northwest of the United States. Phase 8 is associated with a westward shift of extratropical cyclone tracks in the north and central Pacific and a southward shift in the mid-Atlantic.

Cyclone intensity is calculated for the mean averaged pressure that occurs in the center of each cyclone. MJO phase 1 and 2 have large negative anomalies in the North Atlantic Ocean, indicating that cyclones are weakened. Phases 3, 5, and 7 have positive anomalies in the Pacific Ocean, indicating that the cyclones are stronger. Phases 4, 6, and 8 do not appear to have any clear intensity differences. In Guo et al. (2017), the cyclone intensity patterns seem to follow the cyclone frequency patterns. The last metric is accumulated cyclone activity. The accumulated cyclone activity is computed by multiplying the cyclone frequency and the cyclone mean intensity. This variable helps to show the relationship between frequency and intensity more clearly. Guo et al. (2017) found that accumulated cyclone activity has opposing anomalies in a north-south orientation in the northern Pacific for MJO phases 2 and 8. This demonstrates that in phase 2, the cyclone activity is shifted northward while in phase 8 it is the opposite with

the cyclone activity shifted southward more towards the central Pacific. Phase 1 features a large positive anomaly in the northern Pacific very close to the Arctic while phase 6 has a large negative anomaly in that same location. Again, phase 1 and phase 6 cyclone activities are mirror images of each other. Phase 1 shows a northward shift of cyclone activity near Alaska, while phase 6 has the accumulated cyclone activity anomalously low for that area as the activity is primarily in the north central Pacific. The rest of the phases are very noisy with no clear patterns.

Overall, Guo et al. (2017) demonstrated that the MJO impacts extratropical cyclone tracks during boreal winter, including their frequency and intensity. The study indicates that tracking the MJO is useful for predictability of cyclone tracks over North America and in the Pacific and Atlantic oceans.

1.4 MJO Teleconnections & Severe Weather

Impacts

MJO teleconnections can modify extratropical cyclone tracks. The teleconnections often form in the Pacific and disturb the subtropical-jet which affects the mean flow to create anomalous large scale cyclonic and anticyclonic patterns for the United States (Barrett and Gensini, 2013). For example, in Deng et al. (2011), these changes in the mean flow can impact precipitation during boreal winter and based on findings from Baggett et al. (2018), Barrett and Gensini (2013), and Bond and Vecchi (2003), the teleconnection patterns can also affect severe weather outbreaks during the spring.

In addition to affecting the extratropical cyclone tracks, the MJO's teleconnection patterns also affect the cyclone's intensity by interrupting the mean flow (Guo et al., 2017). When cyclone intensity is compared with cyclone frequency, the modulations due to the MJO can be seen more clearly. Guo et al. (2017) found that in the north Pacific, the modulations to the cyclone intensity were due to westerly and easterly wind anomalies in the northern Pacific. As for the cyclones in the sub-tropics, positive and negative moisture anomalies were correlated with cyclone intensity (Chang and Zurita-Gotor 2007). Depending on the directions of the winds in the northern Pacific and the signs of the moisture anomalies in the sub-tropics, these factors determine whether the storm tracks had little modulation due to the counteraction of opposite signs or if the signs were the same and enhanced the track variations (Guo et al., 2017).

Barrett and Gensini (2013) is based off of a previous study by Thompson and Roundy (2013) and uses their hypothesis that the MJO does have an effect on the atmospheric dynamics that create idealized severe weather environments. Barrett and Gensini (2013) studied the impact of the MJO on tornadoes in the central United States (defined as the area between the Rocky Mountains and the Mississippi River) during the spring season (April-May) from 1990-2011. They used tornado data from the Storm Prediction Center that included intensity, location, damages, and time of each tornado. Following the methodology of Gensini and Ashley (2011), they examined 500-hPa geopotential heights, 800-hPa geopotential heights, and mean sea level pressure values of CAPE and SRH. The RMM index was used to measure the intensity and location of MJO convection and only strong events were considered. Tornado likelihood was calculated and a binary statistic test was used to find significance. The study found

that MJO phase 8 was the only phase that had above normal p values for tornado likelihood for the whole spring season. While splitting up the April and May months, April saw below normal tornado days in phases 3-5 and 7 and May saw below normal days during phases 2 and 3. MJO phase 6 provided above normal values for tornadoes in April and phase 5 reported above normal activity for May (Barrett and Gensini, 2013). For a majority of the anomalous tornado days, the environment was very conducive for severe weather with above average CAPE and SRH values. Overall, the CAPE and SRH anomalies matched the tornado likelihood anomalies when composited by MJO phase. When the tornado days were above normal in certain phases, so were the severe weather parameters.

The 500-hPa and 800-hPa geopotential heights and mean sea level pressure were used to study the environment during these tornado events. Barrett and Gensini, (2013) found that negative sea level pressure anomalies occurred west and south of the positive CAPE and SRH anomalies. The 500-hPa and 800-hPa geopotential height anomalies were also located west and south of the severe weather parameter anomalies. Having a low pressure system to the west of the tornadic activity aided the anomalous events due to the influx of southerly flow and moisture. The study suggests that the MJO impacts the environment for tornadogenesis by affecting the midlatitude circulation patterns. Modifying the large-scale circulation leads to a change in the thermodynamics in synoptic scale features. For example, CAPE and SRH values can be intensified depending on the location and intensity of the MJO. The enhancement of the severe weather parameters then leads to an increase in tornado likelihood.

Baggett et al. (2018) examined the impact of the MJO on severe weather in the United States during the spring (March-June) for 1979-2015, with a focus over the Plains and Southeast U.S. regions. The purpose of this study is to determine if the MJO can enhance subseasonal forecasting skill of severe weather activity in the United States. Baggett et al. (2018) followed the methods of Mundhenk et al. (2018) and used a two-class empirical prediction model with lead times of 1-29 days and 500-hPa geopotential heights to test severe weather predictability associated with the MJO. The study used the outgoing longwave radiation (OLR) MJO index (OMI; Kiladis et al., 2014) and examined strong MJO events out to five weeks prior. The model was trained with MJO data for past severe weather outbreaks in the United States to forecast certain severe weather parameters, including hail, tornadoes, storm relative helicity (SRH), convective available potential energy (CAPE), and convective storm relative helicity (CSHR2) which is calculated by $(CAPE \times SRH^2)$. The CAPE and CSHR2 values were acquired from the ERA-Interim reanalysis, and the hail and tornado data from the Storm Prediction Center's Severe Weather Database. The model uses the variable's conditional and climatological distributions and compares their means for each variable. If the conditional mean is greater than or less than the climatological mean, the model will forecast above or below normal for that severe weather parameter, respectively. The model forecast is trained by leaving one year out and verified by comparing it to the observations for that year (i.e. a hindcast). Then, skill is computed from the accuracy of the model compared to the observations for each parameter.

To assist in the explanation of the forecast skill, Baggett et al. (2018) used 500-hPa geopotential height anomalies to get a better understanding of what was happening

in the middle layers of the atmosphere. These 500-hPa geopotential height anomalies create environments favorable for severe weather to occur. The 500-hPa geopotential height anomalies were composited into weekly averages and separated by MJO phase. The location of these anomalies were good indicators of where to expect severe weather in the Plains and Southeast regions because the highest skill correlated with the most anomalous structures. According to Baggett et al. (2018), when the model included the MJO's initial state as opposed to just climatology as a predictor, the model's skill over the plains was the highest when forecasting for tornado and hail. In the southeast U.S., most of the forecasts had lower than average skill scores in all severe weather parameters except SRH (Baggett et al. 2018). The Ohio River Valley appeared to have a lower skill than the rest of the plains. Factors that may affect the MJO skill are jet stream variability, the low-level jet, or even the Great Lakes in that area. Overall, including the MJO lengthened skillful lead times (Baggett et al., 2018). It took about 2 weeks for the MJO teleconnections to reach the Plains/Southeast regions, but according to Baggett et al. (2018), that is also the amount of time it takes for Rossby waves to travel from the tropics to the United States.

This research shows that though MJO teleconnection patterns may have a large amount of variability, they can positively contribute to forecast skill. They can be tracked by geopotential height anomalies and many other variables to study their impacts on U.S. weather in the spring. Using MJO activity as well as other teleconnection patterns as predictors in an empirical prediction model can add skill to a forecast. The current phase of the MJO can be quite telling of the intensity and location of the upcoming

troughs or ridges. Incorporating these teleconnections into forecasts could provide longer lead times for people and businesses to prepare for severe weather events.

Bond and Vecchi (2003) focused on how the MJO affects large-scale dynamics to create favorable environments for flash flooding in the Pacific Northwest during winter. These floods can lead to mudslides, and can be costly due to property damage and lives lost. The MJO's teleconnection patterns can disrupt the large scale mean flow creating anomalies over the northern Pacific Ocean that can lead to severe weather outbreaks such as heavy rain and flooding events. Flooding from three major rivers located in western Washington were examined using stream-flow records from the U.S. Geological Service gauges: the Sauk River, Snoqualmie River, and the Chehalis River, each representing the northern, central, and southern part of the state, respectively. Bond and Vecchi (2003) only examined major flooding events, defined as a magnitude corresponding to a 2-year return period or greater. The two time periods considered from 1979-2000 are October-December (OND) and January-March (JFM). National Centers for Environmental Prediction (NCEP) reanalysis 850-hPa zonal winds and 500-hPa geopotential height were used, as well as the OMI daily MJO indices and a daily rain gauge dataset from Widmann and Bretherton (2000). Then, both of the daily datasets were calculated into monthly climatology datasets.

Each flood event was examined separately. If the MJO was active, they recorded which phase it was in during each flood. Two tests were created to determine how the MJO impacted flooding in the Pacific Northwest. The first test was called "MJO modulation" and focused on the timing of the mean precipitation rate in relation to MJO phase. The second test was named "MJO enhancement" and was representative of the

frequency or mean precipitation rates during active or suppressed MJO activity (Bond and Vecchi, 2003). Starting with the Cascade Mountains and using mean precipitation values over Washington and Oregon as a reference, Bond and Vecchi (2003) noticed the western slope received four times as much precipitation than the eastern slope. During OND, there were higher precipitation amounts for the northern part of the Cascade Mountain range than there were for JFM. For the western slope of the mountains, MJO phase 8 showed 150-200% more precipitation than phase 2. As for both Washington and Oregon, their study found that during OND, MJO phases 7 and 8 coincided with wetter than normal conditions and during MJO phases 1, 2, and 4, drier conditions occurred.

During the late winter season (JFM), precipitation is enhanced during MJO phase and suppressed during phases 2 and 7. The anomalous high and low precipitation were approximately the same magnitude as during OND, with the MJO signal weaker during JFM in western Oregon (Bond and Vecchi, 2003). This could be due to the seasonality of the MJO, since the MJO was more active during OND than during JFM. The MJO was also found to impact flooding of the three selected rivers in Washington. The flooding that occurred happened in at least two out of the three rivers at any given time, indicating that the floods were related to large-scale dynamics as opposed to small convective events. Strong MJO events occurred for more than half of the flooding events during the OND months. MJO phase 7 was associated with most of the flood days while no flood days occurred during MJO phases 1 and 2. During JFM, which experienced less flooding days than OND, the suppression of rainfall was more apparent than its enhancement. There were only slightly more flooding events that

occurred in MJO phases 4 and 5 and the rivers were noticeably drier during phases 6 and 7.

MJO wind anomalies also have a significant effect on precipitation in Oregon and Washington. When the MJO creates anomalous westerlies near the dateline in the southern Pacific, the northwest experiences wetter than normal conditions. When the MJO forces anomalous easterlies near the central Pacific, the Pacific Northwest experiences drier than normal conditions. Bond and Vecchi (2003) examined large-scale circulation patterns using 500-hPa geopotential height. A favorable rainfall pattern for the Pacific Northwest includes a large trough off the west coast and sufficient southwesterly flow. This scenario happened the most in OND during MJO phases 7 and 8. Though phase 4 had a similar set-up to phases 7 and 8, no significant rainfall occurred on the western side of the mountains. Bond and Vecchi (2003) speculated that the reason phase 4 did not produce as much rainfall as expected is due to the trough's proximity to the coast. The trough seemed to stay further away from land and actually suppressed rainfall instead.

Understanding that the MJO has an effect on extratropical large-scale dynamics due to its teleconnections can be an advantage for forecasting in the Pacific Northwest. Overall, the 500-hPa geopotential height anomalies for JFM were on average south or east of the anomalies during OND (Bond and Vecchi, 2003). They speculated this pattern may be due to the seasonality of the subtropical jet. The MJO can be a valuable predictor but one must consider its change in intensity and the other large-scale dynamics that affects its teleconnections.

To understand how the MJO impacts tornadogenesis during May-July, Kim et al. (2020) examined CAPE, low-level wind shear (LLWS), and the deviation from the average tornadogenesis during each MJO phase for each month. The tornadoes (EF1-5) are overlaid on a $1^\circ \times 1^\circ$ grid and are counted in each grid box over the United States. They found that out of the strong MJO days in their time period, about 41% observed EF1-5 tornadoes in the United States. The relationship between MJO phase and tornadogenesis is more favorable during the late spring and early summer months. For March, phase 2 was associated with a favorable environment for tornadoes while for April, it was phases 5 and 8. As a whole, phases 3-6 supported tornadogenesis in the United States while phases 1,2,7, and 8 showed an environment of suppression for tornadoes. Kim et al. (2020) found there were two areas in the United States where tornadogenesis occurred: the South and in the Ohio River Valley during phases 3-4 and the Southeast and Northeast during phases 5-6. Overall, the highest occurrence of tornadogenesis started in the southern United States around the Texas and Oklahoma areas.

Kim et al. (2020) examined the large-scale circulation associated with favorable or unfavorable tornado environments during MJO events, referring to phases 3-6 that enhance tornadogenesis, and phases 1,2,7, and 8 which suppresses it. For the enhancement phases, the MJO creates anomalous ridging in the southern United States which works to enhance the North American Low-Level Jet (NALLJ) and results in increases in LLWS and CAPE values. The suppressing MJO phases create anomalous troughing, resulting in a weaker NALLJ and weaker LLWS and CAPE. Since the severe weather parameters were determined by the location and intensity of the

NALLJ, this parameter was also modulated by the MJO. Kim et al. (2020) further supports that the MJO can impact certain severe weather parameters as well as tornadogenesis in the Ohio River Valley and in the southern region of the United States.

Chapter 2

Methodology

In this analysis, the RMM indices are used to measure the intensity and location of the MJO. The RMM indices are derived from the leading two combined EOFs of OLR and 850-hPa and 200-hPa zonal winds (Wheeler and Hendon 2004). Intraseasonal variability and the annual cycle are removed and the daily observed data are projected onto the EOFs to produce RMM1 and RMM2. Only significant MJO events are included in this study, defined as when $\sqrt{(RMM1)^2 + (RMM2)^2} \geq 1$.

Kevin Hodges' tracking algorithm (Hodges 1999) is applied to mean sea level pressure data from ERA5 reanalysis (Hersbach et al., 2020) (See Fig. 1). Certain constraints were applied to the mean sea level pressure values to filter the data properly in order to find the cyclone centers more easily. Hodges' (1999) method consisted of an upper-bound displacement constraint, velocity constraints, and track smoothness constraints. The cyclone constraints were performed on the data to link together similar minimum mean sea level pressure centers (1013 hPa). The separation of each cyclone track is determined by changes in velocity of the storm in at least three time steps per day (Hodges, 1999). If the time steps start to change velocity, then a new cyclone track is formed. Next, text files are generated containing the cyclone's track length, latitude

and longitude coordinates, and intensity. A smoothing constraint is applied to the minimum mean sea level pressure center points both forward and backwards in time and extra points are added to the beginning and end to any incomplete tracks so that all tracks have the same number of points (Hodges, 1999). Cyclone tracks that are shorter than two days, move less than 5° per day, and are less intense than $13 \times 10^{-5} \text{ s}^{-1}$, are considered weak and short-lived and are excluded from the dataset.

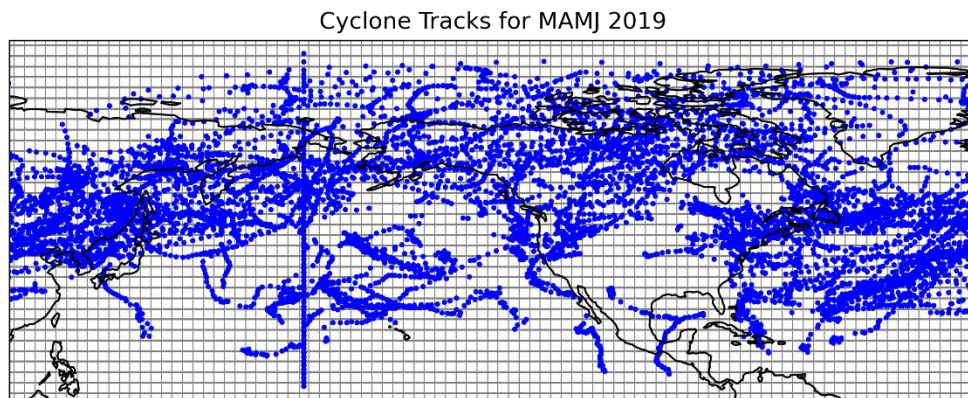


Figure1. Cyclone tracks from Kevin Hodges' (1999) tracking algorithm for MAMJ 2019.

From the storm track data, cyclone frequency is computed and intensity is collected and analyzed according to MJO phase. Cyclone frequency is important when considering how MJO teleconnections affect spring weather. High cyclone frequency indicates where cyclones are most often observed, which is important for understanding regions that often observe severe weather outbreaks or flash flooding events. The Hodges (1999) tracking algorithm is used to collect extratropical cyclone data from 1979-2019 for the months of March-June. Only the cyclone tracks lasting longer than 48

hours with tracks longer than 1000km were used in this analysis, as in Baggett et al. (2018), Guo et al. (2017), and Grise (2013).

Frequency is computed by first compiling the 3-hourly data into daily data. This is done by first counting the number of time steps with a cyclone detected for each day and for each grid box. A daily count was then computed by reducing to only one count if at least one time-step contained a cyclone that day, forming a daily dichotomous index where a 1 indicates a cyclone is present and 0 if there is not. This index is computed for all of the years and then composited by MJO phase using the RMM indices. The mean cyclone frequency (Fig. 1) is computed by summing the cyclone counts and dividing by the total number of days in the spring season (i.e. 123 days) over the 40 years and multiplying by 100 to find a percentage. Cyclone frequency anomalies are computed by subtracting this mean frequency.

Seeing the frequency of the tracks show where extra-tropical cyclones travel the most, but using 500-hPa geopotential height data shows where there are anomalous high and low geopotential height anomalies due to the MJO. ERA5 geopotential height data are composited by MJO phase for MAMJ. The climatological mean was then calculated and taken out of the dataset so that the anomalies were shown. A two-tailed Student's t-test at the 95% significance level was applied to the anomalies.

Cyclone intensity is computed similarly to how frequency is computed except intensity only counts the grid boxes that have storms. Then, a daily dichotomous index is also used for the daily counts of cyclone intensities. The sum of the daily intensities is divided by the counts of the daily cyclone intensities to get the average cyclone intensity per day. The average cyclone intensity is computed for all of the years and is then

composited by MJO phase using the RMM indices. The average cyclone intensity anomalies are computed by subtracting the mean intensity.

Chapter 3

Results

3.1 500-hPa Geopotential Height Anomalies

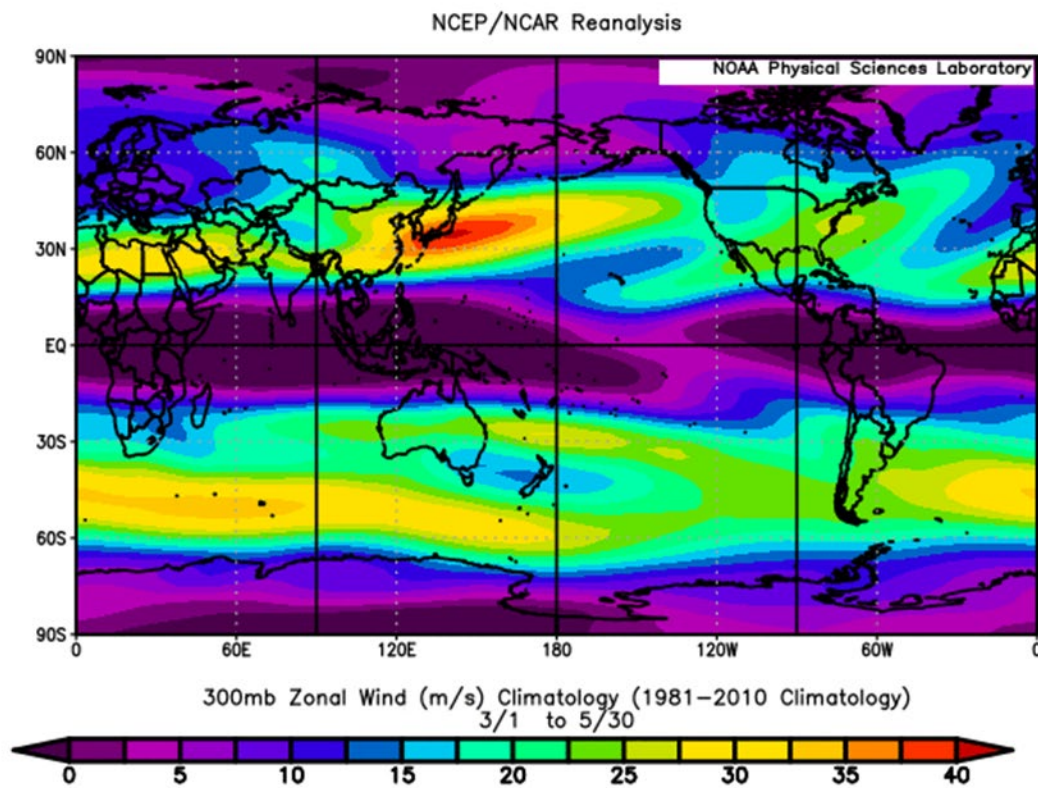


Figure2. NCEP/NCAR Reanalysis 300-hPa geopotential height zonal wind plot for 1981-2010 climatology.

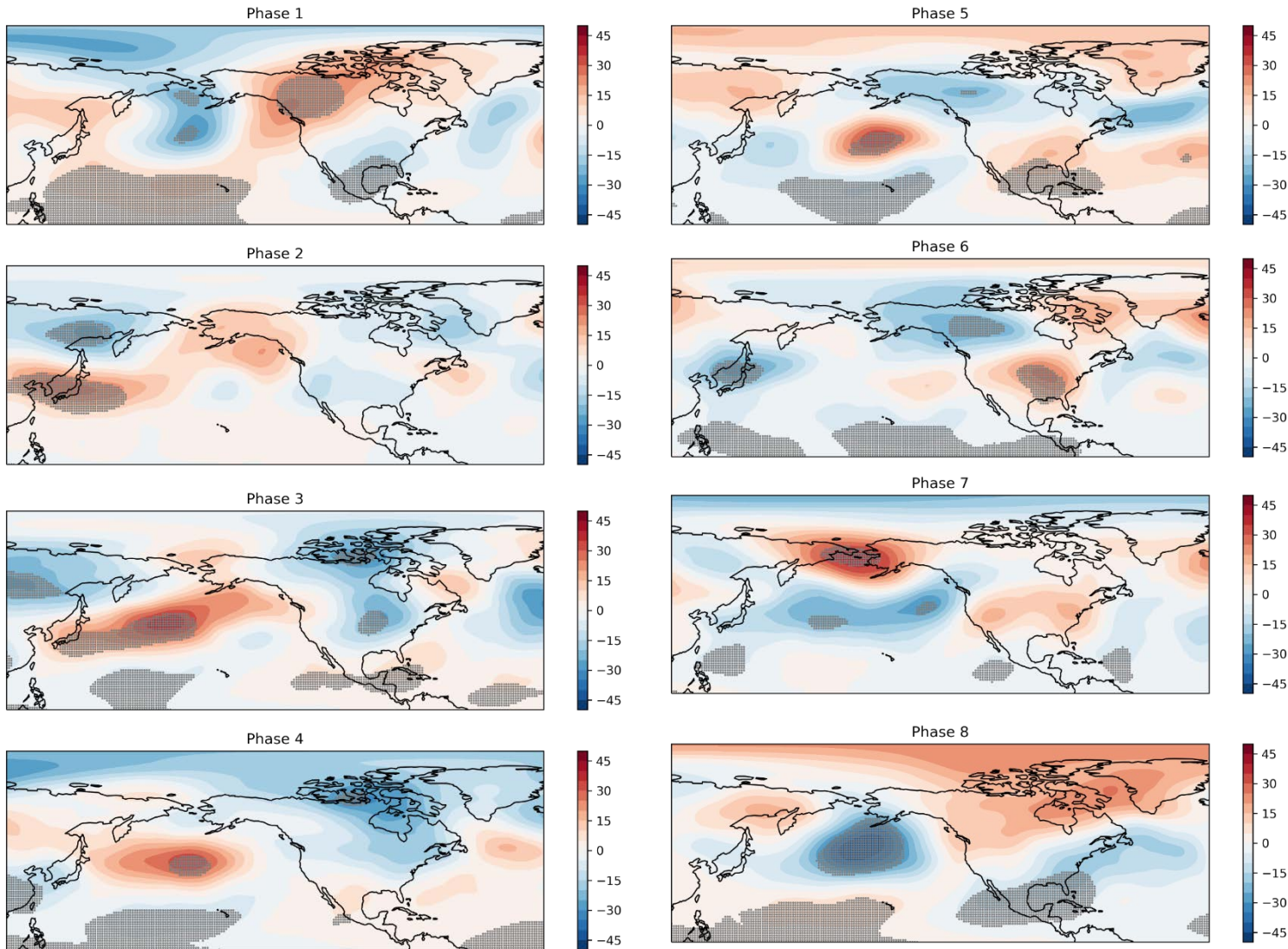


Figure 3. 500-hPa geopotential height anomalies composited by MJO phase during MAMJ 1979-2019. Stippling represents anomalies significantly different from zero at the 95% significance level based on a two-tailed Student's t-test.

Figure 2 shows the mean MAMJ 300-hPa zonal wind for 1981-2010 from the National Centers for Environmental Prediction/ National Center for Atmospheric Research reanalysis data. This figure is included as a reference for the MJO-driven anomalies discussed in this section. During the spring season, the Pacific subtropical jet maximum can be found off the east coast of Asia extending to the northeastern Pacific. Considering the average jet locations makes the MJO's modulations to the jet clearer

when looking at the 500-hPa geopotential height anomalies. A retraction or extension and northward or southward shifts of the jet will affect an extratropical cyclone's tracks.

In Fig. 3, the spring season 500-hPa geopotential height anomalies are composited by MJO phase demonstrating the teleconnections associated with all eight phases. Phases 1, 3, 5, and 6 have significant anomalies over North America, with phase 3 showing one significant anomaly and phases 1, 5, and 6 with a significant dipole structure. Following the phases in order, the eastward propagation of the MJO induced anomalies can be especially seen in phases 2-5. An anomalous anticyclonic anomaly moves eastward as the MJO propagates eastward. The ridge starts in the western Pacific for phase 2 and travels eastward over the central Pacific by phase 5. During phase 6, another anticyclonic anomaly develops over the southern portion of the United States and there are two cyclonic anomalies: one over Alaska and one situated over Japan. As for the transition from phase 7 to phase 8, the cyclonic anomaly starts to get organized in phase 7 and strengthens in the central Pacific in phase 8.

These 500-hPa geopotential heights anomalies disturb the mean flow over the Pacific and North America. This suggests disturbances to the mean jet stream and wavier flow with ridges and troughs. We can expect changes to the zonal flow based on Fig. 3 in comparison to Fig. 2. Based on Fig. 3, we would expect that spring MJO teleconnections will affect extratropical cyclone pathways, frequency, and intensity through transient synoptic eddy activity.

3.2 Frequency Climatology

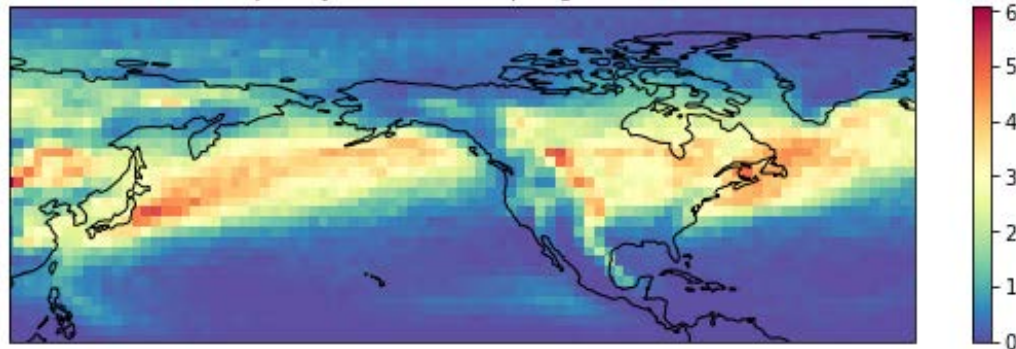


Figure 4. Using the Hodges' (1999) cyclone tracking algorithm, cyclone frequency was computed for MAMJ 1979-2019.

Figure 4 is the boreal spring climatological frequency of cyclone tracks from 1979-2019. The highest frequency of approximately 6% exists off the east coast of Asia near Japan, over the western Atlantic Ocean off the east coast of the United States, and near the Rocky Mountain range. Over North America, cyclone track frequency peaks over northern Canada and off the New England coast into eastern Canada with values between 5-6%. As for the United States, the Central Plains has slightly lower frequencies of about 3-4% but the Rocky Mountain area has higher percentages of frequencies at about 6%. The increase in cyclone frequency anomalies near the Rocky Mountains would suggest the presence of lee-side subsidence (Martin 2006). Overall, the areas of highest cyclone frequency match the areas of highest zonal wind in Fig. 2. This suggests that cyclogenesis occurs over areas with large wind shear (Martin 2006). Large wind shear creates areas of baroclinic instability which are also favorable for cyclogenesis and help to maintain transient synoptic eddy movement downstream (Chang et al., 2002).

3.3 Frequency Composited by MJO Phase

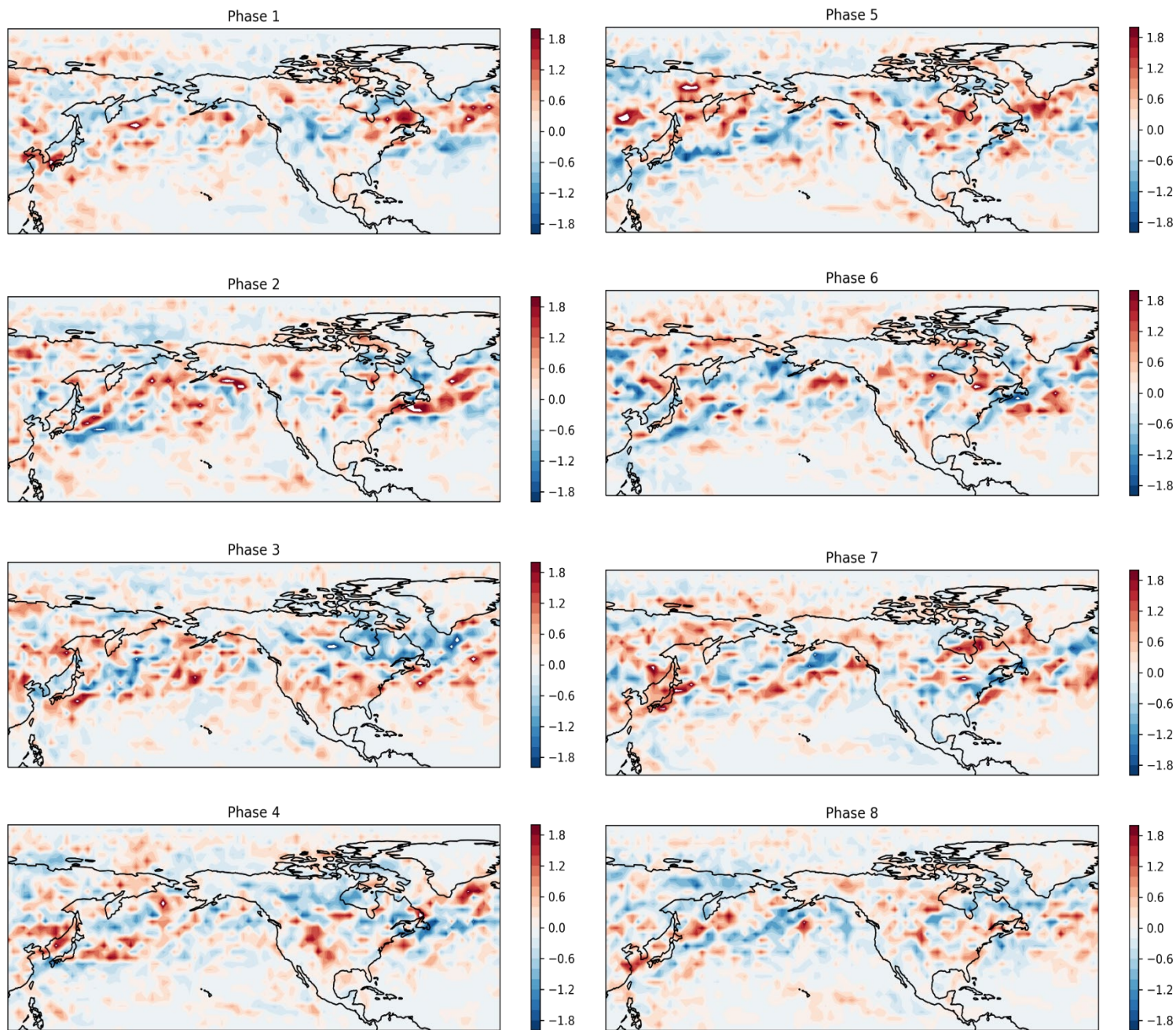


Figure 5. Cyclone frequency separated by MJO phase during MAMJ 1979-2019

Figure 5 shows storm track frequency composited by MJO phase with climatology (i.e. Fig. 4) removed. The figure may appear noisy but there are patterns

that are comparable to the 500-hPa geopotential height anomalies. Phases 1 and 2 experience the highest frequency increase of 1.8% off the northeast coast of the United States while phases 3 and 4 have negative anomalies in the same location with values of about -1.2%. Phase 5 features two locations of high anomalous cyclone frequency of 1.8% in the northwest Pacific just south of Russia and off the northeast coast of North America just west of Greenland. During phase 6, the United States has a slight cyclone frequency increase of about 0.6-1.2% for the western half of the country. Phases 7 and 8 feature their anomalous cyclone behavior over the Central Pacific and off the east coast of Canada. These two phases show opposite-sign anomalies in these locations. Phase 7 has anomalous high frequency, with an increase of about 1.2 to 1.8% for the Central Pacific and off the east coast of Canada while phase 8 has a decrease in frequency of about -0.6 to -1.2% for those areas.

Referring to Fig. 3 phases 1, the large-scale flow in relation to cyclone frequency is particularly modulated over the western United States and in the northern Atlantic Ocean. The positive geopotential height anomaly situated over northern Canada works to block the transient synoptic eddies from traveling through the central United States (Chang et al., 2002). Looking at Fig. 5 phase 1, we can expect to have a decrease in cyclone frequency over the United States which is true with values at about (-0.6 to -1.2%). As for Fig. 3 phase 2, there is another positive geopotential height anomaly near Japan that is the southern portion of a dipole. Looking at Fig. 5 phase 2, we can expect a decrease in cyclone frequency due to the presence of low potential vorticity near the positive geopotential height anomaly. If there are indications of negative potential vorticity in this area, this suggests the left jet entrance region would be situated just

south of where it normally is located. The left entrance region is normally located near Japan (Fig. 2), but in Fig. 5 phase 2, it would be expected to be located near the Philippines instead which would suggest that the dipole behavior forces a southward shift to the large-scale flow.

Switching to the negative geopotential height anomaly perspective, looking at Fig. 3 phase 3, we can see there is an anomalous geopotential height minimum located over the central Plains region of the United States. This disturbance would be expected to have a southward shift the large-scale flow due to the troughing associated with it (Chang et al., 2002). Referring to Fig. 5 phase 3, looking at the United States we can see there are positive frequency anomalies situated over the central United States and negative frequency anomalies over the area near the Labrador Sea. The positive anomalies are centered near the central Plains which is a departure from climatology. For climatology, the anomalies are usually located in the northern Plains near the Canadian border (Fig. 4). These frequency anomalies would suggest that there is a southward shift in frequency when comparing these values to the mean (Fig. 4).

When looking at Fig. 3 phases 3-5 we can see a positive geopotential height anomaly which moves slightly eastward through time in the central Pacific. For Fig. 5, we will group these same phases as well when looking at cyclone frequency anomalies. At first, the positive geopotential height anomaly only slightly affects the cyclone frequency. Since cyclogenesis typically occur in the left exit region of the jet (Martin 2006), this quadrant can be expected to be located in the north central Pacific due to the location of positive cyclone frequency anomalies. Looking at Fig. 5 phases 3 and 4, there are positive frequency anomalies in that area. It is not until phase 5 that the

effects of the persistent positive geopotential height anomaly can be seen on the storm tracks. Focusing on the north central Pacific and the north western Pacific off the east coast of Japan, there are negative frequency anomalies which are opposite values of what was seen in phases 2 and 3. Comparing phase 5 to climatology in Fig. 4, there is a departure from the mean as well as there are normally higher frequencies in the northern Pacific. This would suggest that similar to phase 1, the positive geopotential height anomaly works to inhibit transient eddy movement through those areas (Chang et al., 2002).

Figure 5 phase 6 features negative frequency anomalies over the Labrador Sea which is a departure from the climatological mean (Fig. 4) for that area. Looking at the geopotential height anomalies for that phase (Fig. 3), there is a dipole located over the northern Canada and over the eastern United States with a negative geopotential height anomaly over a positive geopotential height anomaly. The dipole set-up would be expected to have a major impact on the large-scale flow over the United States. However, since the dipole is situated over North America, the effects on the cyclone tracks happen downstream near the Labrador Sea. Comparing these negative frequency anomalies to Fig. 4, we can see these anomalies are a departure from the mean. This suggests the positive geopotential height anomaly inhibits cyclone frequency from occurring in the northern Atlantic due to the presence of negative potential vorticity values over the central United States (Chang et al., 2002).

As for phase 7, the dipole structure is situated north-south with a positive geopotential height anomaly situated north of a negative geopotential height anomaly located in the northern Pacific in the Bering Strait. The location of the positive frequency

anomalies is also an indication of an environment favorable of cyclone activity. The positive frequency anomalies happen to be positioned in the central and central eastern Pacific off the west coast of Canada. These frequency anomalies are slightly south of where they are normally positioned in the northern Pacific in Fig. 4. This would suggest that the dipole structure would enhance the curvature of the flow due to the change in wind shear between the dipoles (Martin 2006). We can also expect the location of high potential vorticity associated with the negative geopotential height anomaly in the central Pacific to be co-located with the left exit region of the jet where cyclogenesis is favorable (Martin 2006). The location of the north-south dipole would not only enhance the curvature of the flow due to the change in wind direction between the dipoles, but also shift the cyclone frequency slightly southward compared to the mean (Fig. 4).

Lastly, referring to Fig. 3 phase 8, a cyclonic geopotential height anomaly is positioned over the central Pacific. The counterclockwise flow disrupts the mean flow by shifting the jet so far southward that it affects the cyclone's ability to form in a favorable environment. Looking at Fig. 5 phase 8 over the central Pacific, there is not much departure from the climatological mean. With the negative geopotential height anomaly, we would expect the cyclone frequency to be shifted to the south as well. However, there is no organized group of positive anomalies in the central Pacific at all. In fact, there are negative frequency anomalies located just north of where the negative geopotential height anomaly would be situated (Fig. 3). The lack of organized anomalous frequency values over the United States is also a departure from the mean (Fig. 4). We can expect this negative geopotential height anomaly to impact the large-

scale flow similarly to a positive geopotential height anomaly and suppress cyclone activity when it is situated in the central Pacific during MAMJ.

3.4 Intensity Climatology

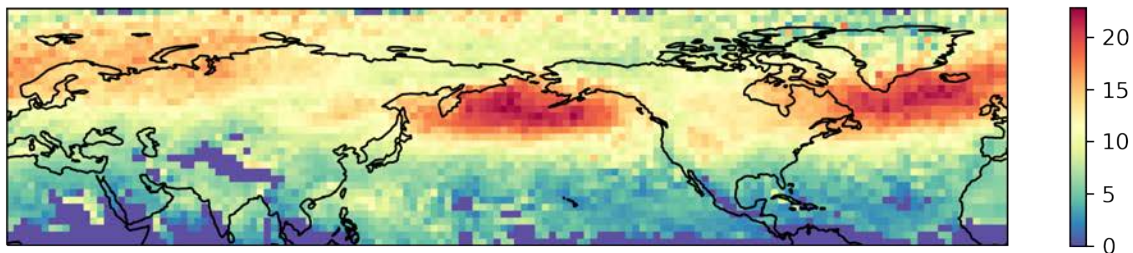


Figure 6. Same as Figure 3 but for cyclone intensity.

Figure 6 is the boreal spring climatological intensity of extratropical cyclones from 1979-2019 using 1013-hPa as the base intensity. The highest intensities of about $20 \times 10^{-5} \text{ s}^{-1}$ occur over the North Pacific and North Atlantic Oceans. It can be inferred that once the cyclones travel over land, their intensities decrease due to friction and topography (Chang et al., 2002). This climatology is geographically similar to cyclone frequency. However, when comparing the climatological intensity (Fig. 6) to the climatological jet (Fig. 2), the intensities are located in the northern Pacific which is slightly north of where the jet max is located. This suggests that the most intense cyclone activity occurs just east of the jet max in the exit region. This result agrees with Chang et al. (2002) in that the strongest cyclone intensity will occur downstream of the area with the strongest baroclinic instability. The strongest area of baroclinic instability occurs near the thermal wind vector in the jet maximum which is situated near Japan (Fig. 2) (Chang et al., 2002).

3.5 Intensity Composited by MJO Phases

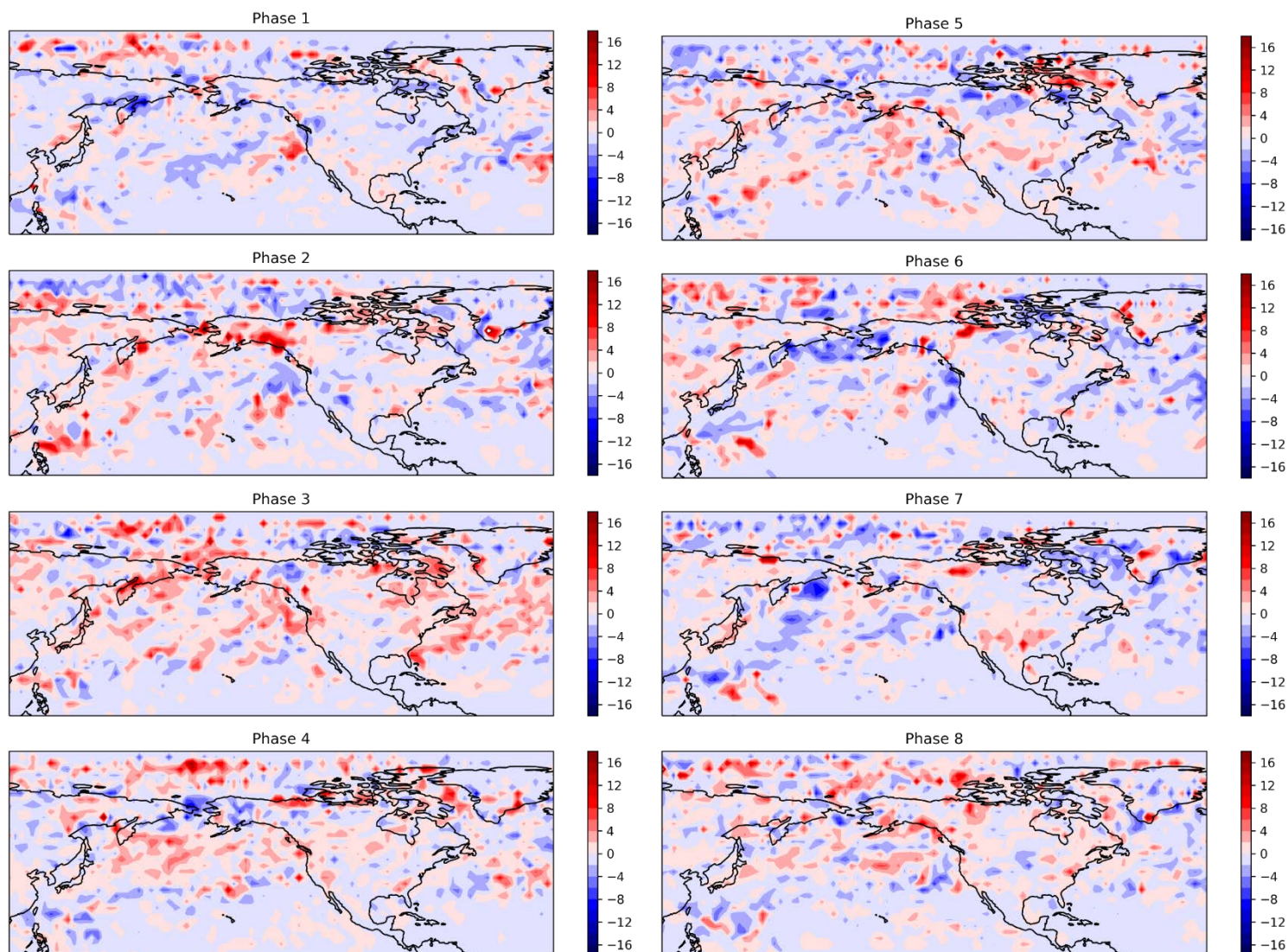


Figure 7. Cyclone intensity separated by MJO phase during MAMJ 1979-2019.

Figure 7 shows cyclone intensity anomalies composited by MJO phase. During MJO phase 1, there are little to no indications of anomalous behavior of cyclone intensity over the central Pacific or northern Atlantic. Phase 1 has negative anomalies of approximately $-4 \times 10^{-5} \text{ s}^{-1}$ in the central Pacific which is a departure from the mean (Fig. 6). For phase 2, positive intensity anomalies ($12 \times 10^{-5} \text{ s}^{-1}$) are situated over Alaska

which matches Fig. 6, but also features a small negative anomaly off the Pacific northwest coast of the United States ($-8 \times 10^{-5} \text{ s}^{-1}$). Phase 3 has the least departure from the mean (Fig. 6) with positive intensity anomalies at approximately 4 to $8 \times 10^{-5} \text{ s}^{-1}$ situated in the central Pacific and northern Atlantic. Phase 4 has positive anomalies in the central Pacific, but has a negative anomaly ($-8 \times 10^{-5} \text{ s}^{-1}$) located in the Bering Strait. This negative anomaly in the Bering Strait is a departure from Fig. 6 where there are normally positive anomalies. Phases 5-7 are the only ones that reflect the slight increase in anomalous intensity at about 4 to $12 \times 10^{-5} \text{ s}^{-1}$ in the western half of the United States. Individually, phase 6 has negative anomalies (-4 to $-12 \times 10^{-5} \text{ s}^{-1}$) over the Bering Strait similarly to phase 4. Phase 7 also has negative anomalous intensity (-4 to $-12 \times 10^{-5} \text{ s}^{-1}$) different than the mean (Fig. 6) just east of Japan extending from northern Russia to southern Asia. Lastly, phase 8 has positive anomalies at about 4 to $6 \times 10^{-5} \text{ s}^{-1}$ over the central Pacific, but they are situated over the east central Pacific.

Considering the behavior of eddy kinetic energy, we can expect the kinetic energy to be enhanced towards the jet exit region due to an increase in baroclinic conversion (Chang et al., 2002). This enhancement of synoptic eddy intensity downstream will modulate the mid-latitude jet stream and can be seen in Fig. 7 by comparing the cyclone intensities to Fig. 3. Looking at Fig. 3 first, phase 1 features a west-east dipole with a negative geopotential height anomaly west of a positive geopotential height anomaly. This would suggest an increase in cyclone intensity where the baroclinic instability is the strongest. Baroclinic instability would be the strongest where there is a strong change in vertical shear (Martin 2006). We can expect a strong vertical wind shear in between the negative and positive geopotential height anomalies

(Fig. 3: phase 1). Phase 1 of Fig. 7 features a positive intensity anomaly south and east of the dipole from Fig. 3. This area just off the Pacific northwest coast of the United States would be where vertical shear is the strongest at the 500-hPa geopotential height level. Referring to Fig. 3 phase 2, there are dipoles but they are situated north-south with a geopotential height minimum north of a geopotential height maximum. The modulation of the large scale dynamics can be inferred to be the same as the set up that appeared in phase 1. Looking at Fig. 7, phase 2, we can expect a positive cyclone intensity anomaly downstream of the flow where the dipoles are located. Phase 2 (Fig. 7) has a positive anomaly over southern Alaska which is downstream and to the east of where the dipoles were located in Fig. 3. The placement of the MJO induced 500-hPa geopotential height anomalies situated in dipoles would suggest that the waviness of the jet is increased compared to the climatological jet (Fig. 2) due to the presence of the dipoles disrupting the mean flow.

Since anticyclones work to diminish cyclone track activity due to low potential vorticity values and easterly flow (indirect circulation) around the anomaly (Martin 2006), we can expect the cyclone intensity to decrease downstream of the geopotential height maximum anomalies. Looking at Fig. 3 phases 3-5, the anticyclone anomaly is situated over the central Pacific. Comparing phases 3-5 to those same phases in Fig. 7, we can expect a decrease in cyclone intensity east of the anticyclone situated over the United States in the exit region of the jet (Chang et al., 2002). This claim is supported with anomalous intensity values of nearly zero in phases 3 and 4 (Fig. 7). Phase 5 is when the intensities start to resemble the mean again (Fig. 6) and has a slight increase in positive intensity anomalies at approximately 4 to $6 \times 10^{-5} \text{ s}^{-1}$ over the western half of the

United States. The presence of this anticyclonic anomaly over the central Pacific suggests a northward modulation of the jet which causes the exit region to be situated over southern Canada and over the northern United States (Fig. 2). Due to the presence of convergence aloft and divergence at the surface in the right jet exit region (Martin 2006), this leads to an unfavorable environment for positive anomalous cyclone intensities downstream of the flow in those areas of North America.

Phase 6 of Fig. 3 shows a dipole located over North America with a negative geopotential height anomaly just north of a positive geopotential height anomaly. Considering the modulation to the large-scale flow in phases 1 and 2, we would expect the cyclone intensity phase 6 (Fig. 7) to show positive anomalies downstream of the flow. However, this is not the case. Switching to Fig. 7 phase 6, we would expect the higher intensity anomaly values to be situated over the northern Atlantic near Greenland and off the east coast of Canada but yet there are no indications of any clear anomalous activity. The lack of any anomalous cyclone intensity activity could be due to the placement of the dipole which is located completely over land. The other dipoles featured in phases 1 and 2 of Fig. 3 had at least one anomaly located over the Pacific Ocean. The dipole anomalies in Fig. 3 phase 6 are also located the farthest east of any other geopotential height anomalies in this figure. Another factor that could inhibit cyclone intensity would be how far away from the jet max these anomalies are located. The transient synoptic eddies will continue to propagate downstream, however, they are the strongest near regions of baroclinic instability which would be near a jet exit region (Chang et al., 2002).

Referring to Fig. 3 phase 7, a geopotential height dipole tries to form near the Bering Strait and northern Atlantic with a positive geopotential height anomaly situated north of a negative geopotential height anomaly. Looking at Fig. 7 phase 7 for cyclone intensities, there is a slight increase in anomalous intensities with a small anomaly in far northern Canada. However, the most impressive anomaly in phase 7 are the negative anomalies just west of the dipole. Negative anomalies are located in the far western Pacific and extend south from the east coast of Russia down to the east coast Asia. There is a small positive intensity anomaly located near the Philippines but this is further south than what climatology shows (Fig. 2). This suggests that the jet is being shifted southward because the intensities will be positive and anomalous in regions of upper-level divergence (Chang et al., 2002).

Lastly, Fig. 3 phase 8 features a negative geopotential height minimum located in the central Pacific. Looking at Fig. 7 phase 8, there are areas of positive intensity anomalies in the eastern Pacific near Alaska and northern Canada. We would expect an increase in cyclone intensity downstream of the negative geopotential height anomaly in the exit region due to the curvature of the jet. This would be referring to the theory that cyclone intensity strengthens near areas of positive vorticity advection in the left exit region of the jet (Martin 2006; Chang et al., 2002).

Chapter 4

Summary & Conclusion

Examining 500-hPa geopotential heights, cyclone frequency, and cyclone intensity in unison gives insight into how large-scale dynamics are affected by MJO teleconnection patterns. The phases discussed above strongly suggest the MJO changes the large-scale circulation during MAMJ through teleconnection patterns. We can expect the teleconnection patterns to change the intensity and location of the storm tracks by changing the intensity and direction of the mean flow. There are many explanations for how the teleconnection patterns will impact the large-scale depending on which phase the MJO is in. Depending on the location of a geopotential height anomaly, whether it is over the ocean or on land, can also have different effects on a cyclone's tracks. If a geopotential height anomaly is located over an ocean, we can expect to see a stronger response to cyclone activity whether it be positive or negative because of an abundance of latent heat release due to condensation in rising air (Chang et al., 2002). The barotropic and baroclinic conversion within the jet is also important when considering how the jet is being modulated by Rossby waves. This conversion is important for the propagation of these eddies and the process can be disturbed by incoming teleconnection patterns. It is important to note that all of the explanations discussed above regarding synoptic eddy behavior work together to disrupt the large-scale flow. Considering the effect of the MJO's teleconnections, we can expect the 500-hPa geopotential height anomalies to disturb the mean flow enough to affect an extratropical cyclone's tracks and intensities.

Currently, less research has been done regarding the spring season and the MJO relative to the winter, when the MJO is stronger and more active. Research on the spring season is important because of the severe weather that is associated with the changes in seasonality during those four months. The lack of MAMJ research was the motivation for this study, in addition to the interesting findings highlighted in the introduction. Applying the results from this study can be beneficial in improving the “predictability gap” in subseasonal timescales, important for increasing lead times for events such as flash flooding or severe weather outbreaks. This study suggests that the monitoring of the MJO would be of significant interest to forecasters due to the fact that its teleconnection patterns affect our large-scale dynamics by modulating the large-scale flow and in turn, extratropical cyclone tracks and cyclone intensity.

Chapter 5

Future Work

Future work includes analyzing the moisture transport associated with the spring MJO teleconnections. Similar to Guo et al. (2017) for the winter season, total column water vapor (TCWV) can be used to track where tropical moisture is transported by the MJO teleconnection anomalies and these can be compared to the cyclone intensities and frequencies. This would allow for a more robust analysis regarding the eastward movement of MJO teleconnection patterns and how moisture is carried from the tropics to the mid-latitudes and how this influences the large-scale flow.

Other methods in addition to Kevin Hodges' tracking algorithm could also be applied to examine extratropical cyclones. For example, Guo et al. (2017) used an eddy variance approach to complement the cyclone tracking algorithm. The eddy variance method allows for the Rossby waves to be tracked and can also show if any Rossby wave breaking occurs. The eddy variance approach would also work well with the TCWV data since Rossby waves are the main source which carries tropical moisture to the mid-latitudes.

Referring to the mid-latitude weather, it would also be beneficial to consider more geopotential height levels than only 500-hPa. Additional levels such as 250-hPa and 800-hPa geopotential heights can provide a more complete look at the teleconnection patterns throughout the depth of the atmosphere. The 500-hPa geopotential height level is sufficient for this study but looking at, say, 250-hPa geopotential height in addition to zonal wind can provide more direct insight into the dynamics of the jet and how it's modulated by MJO phase. Since the jet has a significant impact on large-scale dynamics, it would be interesting to consider how it is shifted or extended/retracted depending on MJO phase during spring. As for the 800-hPa geopotential height level, this perspective is much closer to the surface than 500-hPa geopotential heights and can be useful for analyzing the baroclinicity of the anomalies or if they are primarily barotropic.

References

- Akahori, K., and S. Yoden, 1997: Zonal flow vacillation and bimodality of baroclinic eddy life cycles in a simple global circulation model. *J. Atmos. Sci.*, **54**, 2349–2361.
- Anyamba, E. K., and B. C. Weare (1995), Temporal variability of the 40 – 50-day oscillation in tropical convection, *Int. J. Climatol.*, **15**, 379 – 402.
- Baggett, C. F., Nardi, K. M., Childs, S. J., Zito, S. N., Barnes, E. A., & Maloney, E. D. (2018). Skillful subseasonal forecasts of weekly tornado and hail activity using the Madden-Julian Oscillation. *Journal of Geophysical Research: Atmospheres*, **123**, 12,661–12,675. <https://doi.org/10.1029/2018JD029059>
- Barrett, B. S. & Gensini, V. A. Variability of central United States April–May tornado day likelihood by phase of the Madden-Julian Oscillation. *Geophysical Research Letters*, **40**, 2790–2795 (2013).
- Baxter, S., and S. Nigam, 2013: A subseasonal teleconnection analysis: PNA development and its relationship to the NAO. *J. Climate*, 26, 6733–6741, doi:10.1175/JCLI-D-12-00426.1.
- Bond, N. A. & Vecchi, G. A. The influence of the Madden–Julian oscillation on precipitation in Oregon and Washington. *Weather Forecast.* **18**, 600–613 (2003).
- Chang E (2001) GCM and observational diagnoses of the seasonal and interannual

variations of the Pacific storm track during the cool season. *J Atmos Sci*, **58**:1784–1800. [https://doi.org/10.1175/1520-0469\(2001\)058<1784:GAODOT>2.0.CO;2](https://doi.org/10.1175/1520-0469(2001)058<1784:GAODOT>2.0.CO;2)

Chang E. and P. Zurita-Gotor, 2007: Simulating the seasonal cycle of the Northern Hemisphere storm tracks using idealized nonlinear storm-track models. *J. Atmos. Sci.*, **64**, 2309–2331, doi:10.1175/JAS3957.1.

Chang, E. K. M., S. Lee, and K. L. Swanson, 2002: Storm track dynamics. *J. Climate*, **15**, 2163–2183.

Chang, P., L. Ji, H. Li, and M. Flugel (1996), Chaotic dynamics versus stochastic processes in El Niño – Southern Oscillation in coupled ocean-atmosphere models, *Physica D*, **98**, 301 – 320.

Chen, G., & Wang, B. (2018). Effects of enhanced front walker cell on the eastward propagation of the MJO. *Journal of Climate*, **31**, 7719–7738. <https://doi.org/10.1175/jcli-d-17-0383.1>

Chen, T. C., and J. M. Chen (1997), On the relationship between the streamfunction and velocity potential of the Madden-Julian Oscillation, *J. Atmos. Sci.*, **54**, 679 – 685.

Climate Prediction Center Internet Team. Climate Prediction Center – North Atlantic Oscillation (NAO), NOAA Climate Prediction Center, 10 Jan. 2012, www.cpc.ncep.noaa.gov/data/teledoc/nao.shtml.

Climate Prediction Center Internet Team. Climate Prediction Center - Pacific/North

American (PNA), NOAA Climate Prediction Center, 10 Jan. 2012,

www.cpc.ncep.noaa.gov/data/teledoc/pna.shtml.

Deng, Y. & Jiang, T. Y. Intraseasonal modulation of the North Pacific storm track by tropical convection in boreal winter. *J. Clim.*, **24**, 1122–1137 (2011).

Esler, J. G., and P. H. Haynes, 1999: Baroclinic wave breaking and the internal variability of the tropospheric circulation. *J. Atmos. Sci.*, **56**, 4014–4031.

Gensini, V. A., and W. S. Ashley (2011), Climatology of potentially severe convective environments from the North American regional reanalysis, *Electronic J. Severe Storms Meteor.*, **6**, 1–40.

Grise, K. M., Son, S. W., and Gyakum, J. R., 2013, "Intraseasonal and Interannual Variability in North American Storm Tracks and Its Relationship to Equatorial Pacific Variability," *Mon. Weather Rev.*, **141**(10), pp. 3610–3625.

Guo, Y., Shinoda, T., Lin, J. and Chang, E.K.M. (2017) Variations of northern hemisphere storm track and extratropical cyclone activity associated with the Madden-Julian oscillation. *Journal of Climate*, **30**, 4799–4818.

Henderson, S. A., Maloney, E. D. & Barnes, E. A. The influence of the Madden–Julian Oscillation on northern hemisphere winter blocking. *J. Clim.* **29**, 4597–4616 (2016).

Hendon, H. H., C. Zhang, and J. D. Glick (1999), Interannual variation of the Madden-Julian Oscillation during Austral summer, *J. Clim.*, **12**, 2538 – 2550.

Hodges, K. I. (1999). Adaptive constraints for feature tracking. *Monthly Weather Review*, **127**, 1362–1373.

[https://doi.org/10.1175/15200493\(1999\)127<1362:acfft>2.0.co;2](https://doi.org/10.1175/15200493(1999)127<1362:acfft>2.0.co;2)

Hurrell, J. W., 1995: Decadal trends in the North Atlantic Oscillation: Regional temperatures and precipitation. *Science*, **269**, 676–679.

Hurrell JW, Kushnir Y, Ottersen G, Visbeck M. 2003. An overview of the North Atlantic Oscillation. In *The North Atlantic Oscillation, Climate Significance and Environmental Impact*, Geophysical Monograph 134, Hurrell JW, Kushnir Y, Ottersen G, Visbeck M (eds). *American Geophysical Union: Washington, DC*; 1–35.

Kim, D., Kug, J.-S., & Sobel, A. H. (2014). Propagating versus nonpropagating Madden–Julian Oscillation events. *Journal of Climate*, 27, 111–125.
<https://doi.org/10.1175/JCLI-D-13-00084>

Kim, D., Lee, S.-K., & Lopez, H. (2020). Madden-Julian Oscillation-induced suppression of northeast Pacific convection increases U.S. tornadogenesis. *Journal of Climate*, **33**(11), 4927–4939. <https://doi.org/10.1175/JCLI-D-19-0992.1>

Knutson, R. R., K. M. Weickmann, and J. E. Kutzbach (1986), Global-scale

intraseasonal oscillations of outgoing longwave radiation and 250 mb zonal wind during Northern Hemisphere summer, *Mon. Weather Rev.*, **114**, 605 – 623.

Knutson, T. R., and K. M. Weickmann (1987), 30 – 60 day atmospheric oscillations: Composite life cycles of convection and circulation anomalies, *Mon. Weather Rev.*, **115**, 1407 – 1436.

Lyu, M., Jiang, X., Wu, Z., Kim, D., & Adames, Á. F. (2021). Zonal-scale of the Madden-Julian Oscillation and its propagation speed on the interannual time-scale. *Geophysical Research Letters*, **48**, e2020GL091239.
<https://doi.org/10.1029/2020GL091239>

Madden, R. A., & Julian, P. R. (1972). Description of global-scale circulation cells in the tropics with a 40–50 day period. *Journal of the Atmospheric Sciences*, **29**, 1109–1123. [https://doi.org/10.1175/1520-0469\(1972\)029<1109:DOGSCC>2.0.CO;2](https://doi.org/10.1175/1520-0469(1972)029<1109:DOGSCC>2.0.CO;2)

Maloney, E. D., and J. T. Kiehl (2002), MJO related SST variations over the tropical eastern Pacific during Northern Hemisphere summer, *J. Clim.*, **15**, 675 – 689.

Martin, Jonathan E. Mid-Latitude Atmospheric Dynamics: A First Course. John Wiley & Sons, 2006.

Moore, R. W., , O. Martius, , and T. Spengler, 2010: The modulation of the subtropical and extratropical atmosphere in the Pacific basin in response to the Madden-Julian oscillation. *Mon. Wea. Rev.*, **138**, 2761–2779, doi:10.1175/2010MWR3194.1.

- Penland, C. (1996), A stochastic model of IndoPacific sea surface temperature anomalies, *Physica D*, **98**, 534 – 558.
- Riviere, G., 2009: Effect of latitudinal variations in low-level baroclinicity on eddy life cycles and upper-tropospheric wave-breaking processes. *J. Atmos. Sci.*, **66**, 1569–1592.
- Sperber, K. E. Taylor, M. F. Wehner, and S. L. Thompson (2003), High-resolution simulation of global climate, part 1: Present climate, *Clim. Dyn.*, **21**, 371 – 390.
- Straub, K. H., and G. N. Kiladis (2002), Observations of a convectively coupled Kelvin wave in the eastern Pacific ITCZ, *J. Atmos. Sci.*, **59**, 30 – 53.
- Thompson, D. B., and P. E. Roundy (2013), The relationship between the Madden-Julian Oscillation and U.S. violent tornado outbreaks in the spring, *Mon. Weather Rev.*, early online release, doi:<http://dx.doi.org/10.1175/MWR-D-12-00173.1>.
- Weickmann, K. M., G. R. Lussky, and J. E. Kutzbach (1985), Intraseasonal (30 – 60 day) fluctuations of outgoing longwave radiation and 250 mb stream function during northern winter, *Mon. Weather Rev.*, **113**, 941 – 961.
- Wheeler, M. C. & Hendon, H. H. An all-season real-time multivariate MJO index: development of an index for monitoring and prediction. *Mon. Weather Rev.* **132**, 1917–1932 (2004).
- Wheeler, M., and G. N. Kiladis (1999), Convectively coupled equatorial waves: Analysis

of clouds and temperature in the wavenumber-frequency domain, *J. Atmos. Sci.*, **56**, 374 – 399.

Zhang, C. D. (2005). Madden-Julian oscillation. *Reviews of Geophysics*, **43**, RG2003.

<https://doi.org/10.1029/2004RG000158>

Zhou, S., L'Heureux, M., Weaver, S. et al. A composite study of the MJO influence on the surface air temperature and precipitation over the Continental United States.

Clim Dyn, **38**, 1459–1471 (2012). <https://doi.org/10.1007/s00382-011-1001-9>